Composites Part A 120 (2019) 116–126

Contents lists available at ScienceDirect

Composites Part A

journal homepage: www.elsevier.com/locate/compositesa

Mechanical and electrical properties of graphene and carbon nanotube reinforced epoxy adhesives: Experimental and numerical analysis

Sensen Han[a], Qingshi Meng[a,*], Sherif Araby[a,b,c,*], Tianqing Liu[d], Murat Demiral[b]

[a] College of Aerospace Engineering, Shenyang Aerospace University, Shenyang 110136, China
[b] College of Engineering and Technology, American University of the Middle East, Kuwait
[c] School of Engineering, University of South Australia, SA 5095, Australia
[d] QIMR Berghofer Medical Research Institute, Brisbane, Queensland 4006, Australia

ARTICLE INFO

Keywords:
Graphene
Carbon nanotube
Nanocomposite adhesive
Electrical conductivity

ABSTRACT

Carbon nanomaterials secure promises of incorporating exceptional mechanical performance and multifunctional properties into polymers. However, questions concerning type of carbon nanofiller, fraction and corresponding change in relevant property are yet to be answered. In this study, graphene platelets (GnPs) and carbon nanotubes (CNTs) were added individually into epoxy adhesive and corresponding structure-property relations were investigated experimentally and numerically. The study shows that: at fractions < 0.25 vol%, GnPs perform better in Young's modulus, lap shear strength and energy release rate compared to CNTs; while CNT-based epoxy adhesives exhibit high increments at fractions > 0.25 vol%. The mechanical performance of the single lap joint specimens with different nanocomposite adhesive were further investigated using 3D finite element analysis. The numerical analysis not only confirms the outcomes of the experiments but also shows that the failures in the nanocomposite adhesive layers occurred due to Mode II failure. Electrical conductivity measurements of epoxy nanocomposite adhesives showed lower percolation threshold (0.54 vol%) for epoxy/CNT nanocomposite adhesive compared to 0.63 vol% when GnPs were used. The contrast in the geometrical structure between GnP (plate-like structure) and CNT (tube-like structure) is crucially responsible for epoxy nanocomposite adhesives' properties. This research pointed out that selecting a carbon filler for a polymer composite is key-factor to determine the end-product function.

1. Introduction

Epoxy resin, as one of the most important structural adhesives, was widespread used in aerospace, automotive, electronics, civil and packaging industries. However, many of these applications require enhanced strength as well as multifunctional properties. Plethora studies attempted to obtain multifunctional epoxy adhesives by mixing epoxy with a second phase such as carbon-based nanofillers including carbon nanotubes (CNTs) and graphene, and their combination [1–4]. Carbon-based nanofillers proved their capabilities to improve strength, toughness, electrical conductivity and other functional performance of epoxy resins [5] owing to their exceptional mechanical and physical properties [6–8] and high specific surface area and aspect ratios [9,10].

Carbon nanotube regarded as a one-dimensional (1D) tube exhibits excellent mechanical properties and high aspect ratio ranging from 30 to thousands [11–13]. Its unique mechanical and physical properties made it attractive as reinforcing filler to develop superior composite adhesives. Graphene, a two-dimensional (2D) allotrope of carbon, has attracted exceptional attention from academia, opening a new era of 2D, plate-like carbon nanomaterials since 2004 [14]. Graphene possesses outstanding specific surface area [15] and superb mechanical and electrical properties [16]. This gives graphene the advantage over other carbon allotropes to develop multifunctional and structural reinforced composites [17,18].

A significant number of articles are available in literature regarding mechanical, thermal, electrical, and thermomechanical properties of CNT or graphene-based epoxy adhesives [19–26]. Despite their mechanical and physical properties are more or less similar, the behavior of CNT and graphene and their interaction with polymer matrix are diverse due to the contrast in morphology. At the nanoscale range, morphologies become very significant in defining the behavior of a material compared to their bulk counterparts. Therefore, it is highly

* Corresponding authors at: College of Aerospace Engineering, Shenyang Aerospace University, Shenyang, 110136, China (Q. Meng). College of Engineering and Technology, American University of the Middle East, Kuwait (S. Araby).
E-mail addresses: mengqingshi@hotmail.com (Q. Meng), Sherif.Gouda@aum.edu.kw (S. Araby).

https://doi.org/10.1016/j.compositesa.2019.02.027
Received 6 December 2018; Received in revised form 20 February 2019; Accepted 27 February 2019
Available online 28 February 2019
1359-835X/

possible that graphene and CNT show their best effectiveness as reinforcing filler in a polymer at different volume fractions [27,28]. This requires comparative analysis of their efficiency as reinforcing filler at range of fractions providing that fabrication process of polymer composites follows identical procedures. In the current work, we used graphene platelet and carbon nanotube as multifunctional-second phase in epoxy adhesives.

It well known that dispersion quality and interface strength between filler and matrix are key factors to determine the composite properties. This explains the enormous number of studies available regarding promoting filler-matrix interface. Generally, graphene and carbon nanotube are chemically modified to promote both dispersion and interface strength; graphene oxide was modified with 1,3,5-triglycidylisocyanurate and incorporated into novolac epoxy [29]. Modified graphene-based composites displays glass transition temperature of 222^{0}C with 90^{0}C higher than the unmodified one [29]. In another study [30], graphene oxide was prepared and covalently modified via Bingel reaction and then added to epoxy resin; the modified graphene-based composites shows 22% increase in flexural strength by only adding 0.1 wt%. Similar trend has been obtained when carbon nanotubes were modified. However, modification process is complex, lengthy and difficult to control. For example, it took ~135 hrs to obtain modified graphene via Bingel reaction involving lots of concentrated acids and other strong chemicals [30]. Furthermore, covalent modification may cause serious damage of graphene integrity, and loss of its conductive properties [27]; it may pose a barrier to electrical conductivity giving high percolation threshold.

In comparison, the yielded graphene platelets (GnPs) features high structural integrity leading to high electrical conductivity of 1460 S·cm^{-1} [31]; range of thickness 3–5 nm offering large surface area giving good interface for stress, heat and electron transfer with epoxy matrix. It is studied that our GnP [31] has epoxide groups existing on the surface which can chemically react with the end-amine groups of epoxy building strong interface for the nanocomposite adhesives; and most important cost-effectiveness (~$20/kg). Taking into account the conditions of preparation of graphene oxide and reduction then modification processes, we believe the GnPs and CNTs −that used in this study − optimize both end-product performance and fabrication process.

Although there are many articles study CNT- or graphene-based epoxy nanocomposites, it is hard to conduct a comparative view on their reinforcing efficacy because the compositions, fabrication techniques and/or processing conditions vary widely from case to case. These factors are crucial in determining the final properties of the composite. Ghaleb et al. [32] fabricated graphene and multi-walled CNT filled epoxy thin-film composites using ultrasonication and spin coating technique. The effect of filler loading (0.1–1 vol%) and sonication time (10, 20, and 30 min) on tensile and electrical properties were studied. The epoxy/graphene composites were tested for different sonication time, while multi-walled carbon nanotubes (MWCNT) for only 20 min where comparative analysis is not applicable. Also, this study did not show reinforcement when graphene or MWCNT were added into epoxy; in fact, the Young's modulus and strength of epoxy composites dropped. The other few studies are on hybrid mixtures of the nanofillers [27,33–37]. Furthermore, no justification was provided in the literature about the reasons to add a nanofiller at a certain content. Thus, it is difficult to conclude from those studies the optimum content of CNTs and graphene to achieve the best mechanical performance and electrical conductivity of epoxy nanocomposites or epoxy adhesives. Fracture toughness, lap shear strength and electrical properties are crucial properties of epoxy adhesives in structural application which were not fully elaborated in the literature. Further, in all the previous studies, the outcomes are often contradictory where it becomes vague to carry out a comparison between CNT or graphene/epoxy composite adhesives. The outcome of our study would provide researchers with a knowledgebase to understand the behavior of each filler and decide which one is suitable for a certain application. For example, in some applications electrically conductive epoxy adhesive is demanded such as electronic packaging while in construction application high mechanical performance is needed.

Considering the aforementioned facts, the effect of individual addition of graphene platelets and carbon nanotube in epoxy adhesives at a range of nanofiller content (0.05–0.5 vol%) has been investigated in this study. Graphene platelets (GnPs), consisting of few graphene layers (1–4 layers), are scalable in production with little decline in mechanical and electrical properties compare to graphene [31]. The obtained results are thoroughly analyzed to comprehend the individual effect of each of these nanofillers, that is, CNTs and GnPs, on the performance of the composite adhesives during service in structural applications. Additionally, numerical analyses were conducted to simulate the behavior of nanocomposite adhesives with different fractions of nanoparticles in a single lap joint. The conclusions achieved in this study will be beneficial for materials scientists and engineers to design and tune their end-epoxy adhesive to suite a certain application.

2. Experiments

2.1. Materials

Graphite intercalation compound (GIC, Asbury 1395) was supplied by Asbury Carbons, Asbury, NJ, USA. Multi-walled CNTs (8–15 nm ddiameter, ~50 μm length, and 98% purity) were provided by the Chengdu Organic Chemicals Pty Ltd., Chinese Academy of Sciences, and its intrinsic electrical conductivity > 100 S/cm. Epoxy – diglycidyl ether of bisphenol A (WSR618, 184–200 g per equiv., denoted E-51) – were purchased from Nantong Xingchen Synthetic Material. Hardener, Jeffaimne D 230 (denoted J230) was supplied by Huntsman, China.

2.2. Fabrication of nanocomposite adhesives

Graphene platelets (GnPs) is fabricated via thermal shocking and ultrasonication; details are elsewhere [38]. Epoxy/GnP nanocomposite adhesives were prepared as follow: GnPs were suspended in acetone and magnetically stirred for 20 min in a metal container. The suspension is then treated ultrasonically for 60 min below 25 °C. Epoxy (E-51) was fully dissolved into the GnPs suspension by magnetically stirring for 20 min followed by sonication under 25 °C for 30 min. Then, acetone was evaporated at 70 °C using hotplate and magnetic stirring. Bubbles and traces of acetone were completely removed from the mixture by vacuum degassing at 100 °C. After cooling down the mixture to 30 °C, the hardener–J230 was added, and manually stirred for 5 min. This produced epoxy/GnP nanocomposite adhesives. The epoxy/CNT nanocomposite adhesives were prepared following the same procedures.

2.3. Characterizations

2.3.1. Morphology

Scanning electron microscopy (SEM, Philips XL30 Feg,) was employed to image the surface texture of the expanded product. Also, SEM was used to examine the fracture surfaces of the lap shear specimens. A thin layer of platinum coated the fractured surface then the SEM imaging was carried out at accelerating voltage of 5 kV.

Morphology of GnPs and CNTs was examined by transmission electron microscopy using (Philips CM200, TEM) at an accelerating voltage of 200 kV. In a controlled sequential procedure, 1 wt% of GnP or CNT in acetone was diluted to 0.0004 wt% to avoid GnPs stacking or CNTs agglomerating. Then, the 0.0004 wt% suspension was dropped on 200-mesh copper grids, followed by drying in a 60 °C fan oven. Dispersion quality of GnP-based and CNT-based composites was imaged using (Philips CM200, TEM) at low fraction 0.125 vol% and high fraction 0.5 vol%.

2.3.2. Mechanical and adhesive tests

Silicone rubber molds were used to prepared dumbbell samples. After blending GnP or CNT/epoxy mixture with hardener and degassing, the nanocomposites were poured into the molds, cured in a fan oven at 80 °C for 2 h then 120 °C for 10 h. Both sides of samples were polished by fine sand paper to suppress visible marks. Then the samples were thermally treated at 100 °C for 60 min to lessen any flaws resulting from polishing. Tensile testing was carried out at a cross-head speed of 0.5 mm/min at room temperature using an XIANGMIN machine. An extensometer (XM-DZSC001) was installed to capture accurate displacement data to measure Young's modulus; all Young's modulus was calculated at strain range 0.05–0.15%.

The toughness of the neat epoxy and nanocomposite adhesives were measured by double cantilever beam (DCB) testing. The adherends (150 × 10 × 10 mm) were fabricated according to ASTM: 3433–99 (2012) and ISO 25217:2009. Copper shims of 0.3 mm in thickness were used to control the adhesive thickness and a non-sticky paper (40-μm thick) was employed to form initial pre-crack. The fracture toughness (K_{IC}) of the neat epoxy and its bulk nanocomposites was measured using compact tension (CT) test following ISO 13,586 standard. The CT sample has dimensions of 30 × 30 × (5–6) mm.

The nanocomposite adhesives were carefully degassed in a vacuum oven for 10 min to remove bubbles, followed by applying adhesives on the substrate's surfaces. These two substrates were bonded by curing at 80 °C for 2 h, then 120 °C for 10 h. The lap shear strength of neat epoxy and nanocomposite adhesives were measured by tensile testing. The adherends (100 × 25 × 1.6 mm) of lap shear test were fabricated according to ISO 4587:2003.

2.3.3. Electrical conductivity

The electrical conductivity of GnPs was measured using a Hall Effect system with four probes, which was tailored by Suzhou Institute of Nano-Tech and Nano-Bionics, Chinese Academy of Sciences. In brief, four probes were positioned with intimate surface which in contact with a test piece, exactly at the four points of a square. After four current–voltage curves were tested to confirm the good contact between the probes and test coupon surface, resistivity measurement was carried out. The electrical conductivity of GnPs was calculated using the entered thickness value.

The electrical resistivity of epoxy nanocomposites was measured using Agilent 4339B high resistivity meter equipped with a 16008B resistivity cell (two-point-probe) at room temperature. The measurement was conducted on the samples of 6.8 mm in thickness and 24 mm in diameter, in accordance to ASTM D257-99. The presented data is the average of at least three measurements.

3. Results and discussion

3.1. Morphology of GnPs and CNTs

Fig. 1 contains transmission electron microscopic (TEM) images of GnPs and CNTs at high magnification. Image (a) confirms that graphite intercalated compounds exfoliate via thermal shock and ultrasonication into graphene sheets constituting few layers (2–5) staked together (yellow arrows) and few single sheets (red arrows). Pieces of sheets are found sitting on lacey carbon support, clearly illustrating flake-like structures; note the wrinkled texture of the GnP's surface is a result of thermal treatment during the production process. This would play an important role in enhancing mechanical interlocking and load transfer between the matrix and GnPs. Image (b) shows the TEM of CNT dropped from aqueous solution. The individual existence of CNT in the TEM image confirms its well dispersion and disentanglement features. The uniform dispersion of CNTs is a key factor to develop electrically conductive nanocomposite adhesive with high mechanical performance.

Since it is believed that thermal expansion changes the surface texture of the expanded product and ultimately the graphene platelets, SEM imaging has been conducted to examine the GnPs' surface. Fig. 2 presents SEM images of the expanded product which yielded after thermally treating graphite intercalated compounds (GICs) at 700 °C for one minute. At low magnification, image (a) shows corrugated and wrinkled surface of the expanded product due to thermal treatment (blue arrows) and number of pores. Randomly regions where selected and magnified in images b, c and d. They confirm and provide clear views of rough edges at microscale (image b and c) and nanoscale (image d) depicted by brown ellipses. Further processing using ultrasonication for one hour exfoliates this expanded product into graphene platelets where the corrugated surface will be maintained and most likely the ultrasonic waves will produce rougher edges. Such rough and wrinkled surface assists the physical interference and mechanical interlocking between GnPs and epoxy resin promoting the mechanical performance of the composites.

3.2. Mechanical properties (experimental analysis)

Quasi-static tensile testing was carried out on dumbbell samples of epoxy/GnP and epoxy/CNT composites and analytical and numerical interpretations were conducted to understand reinforcing mechanism of each filler. The Young's modulus of both types of composites is calculated from the slope of initial straight portion at strain range 0.05–0.15% and presented in Fig. 3a. Tensile strength is determined at the maximum stress obtained during tensile testing and shown in Fig. 3b. The results reveal that Young's modulus and tensile strength are initially improved with the addition of GnPs or CNTs but at different increments. In Fig. 3a, at fractions < 0.25 vol%, the reinforcing effect

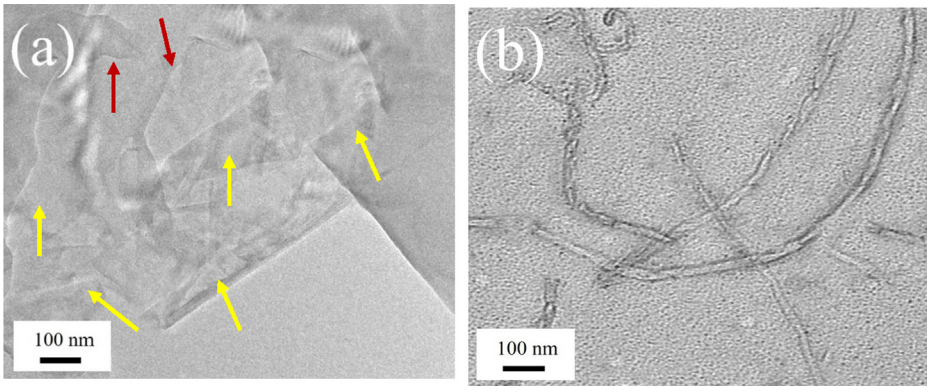

Fig. 1. TEM images of (a) graphene platelets and (b) multi-walled carbon nanotubes.

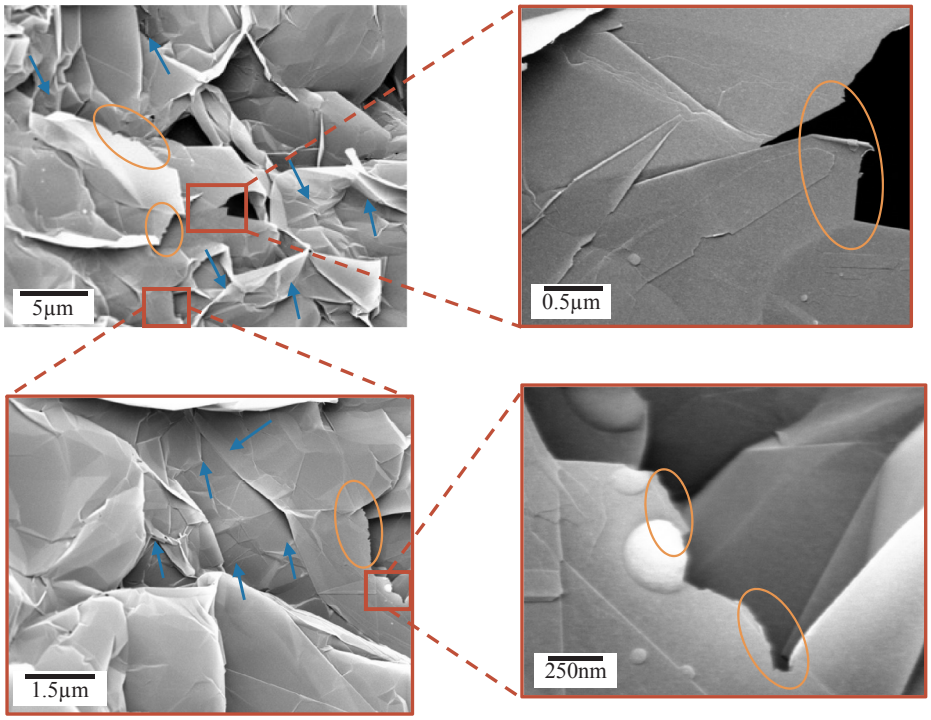

Fig. 2. SEM images of the expanded product after thermal shocking at 700°C.

of GnPs is higher than that of CNTs; for example, at 0.05 vol%, Young's moduli of epoxy/GnP and epoxy/CNT are 2.1 GPa and 1.75 GPa, respectively. It follows similar trend at filler content of 0.125 vol%. Beyond 0.25 vol%, the reinforcing efficacy is swapped to CNTs; at 0.5 vol %, CNTs denoted 80% improvement in Young's modulus while GnP's system exhibited an increase of 68% at the same fraction. In Fig. 3b, tensile strength displayed maximum enhancement of 20% at 0.125 vol % in case of GnPs and 23% in case of CNTs; then tensile strength for both nanocomposite systems experience degradation with faster rate in case of GnPs. In fact, above 0.25 vol% of filler, the tensile strength became less than that of neat epoxy adhesive.

Lap shear strength and adhesive toughness (energy release rate, G_{IC}) as a function of filler content are plotted in Fig. 4a&b, respectively. At all fractions, both GnPs and CNTs augment the lap shear strength and adhesive toughness compared to the neat epoxy adhesive. For example, at 0.5 vol%, lap shear strength and G_{IC} increased, respectively, by 22% and 195% when GnPs is added, and 25% and 231% in case of CNTs. Also, it is concluded from Fig. 4 that filler content determines the enhancement efficiency; at fractions < 0.2 vol%, GnPs promote the adhesive properties at higher increment compared to CNTs. For example, at 0.05 vol%, lap shear strength and toughness increased by ~ 10% and 100% for GnPs while it increased by ~ 3% and ~ 40% in case of CNTs, respectively.

Fracture toughness (K_{1C}) of both nanocomposites (epoxy/GnP and epoxy/CNT–bulk samples) was tested using compact tension samples and results are plotted in Fig. 4c. Results of fracture toughness show similar trend which observed in critical energy release rate (G_{IC})–Fig. 4b. From Fig. 4c, both CNTs and GnPs enhance the fracture toughness of epoxy; at 0.5 vol%, fracture toughness increased by 163% and ~200% when GnPs and CNTs are added respectively. It is obvious that GnPs perform better with the epoxy compare to CNTs at low fractions (< 0.2 vol%) which also concluded in critical energy release rate G_{IC}.

Evidently, these results suggest that there is a critical filler concentration after which the Young's modulus, tensile strength, lap shear strength and energy release rate (G_{1C}) of the nanocomposite adhesives

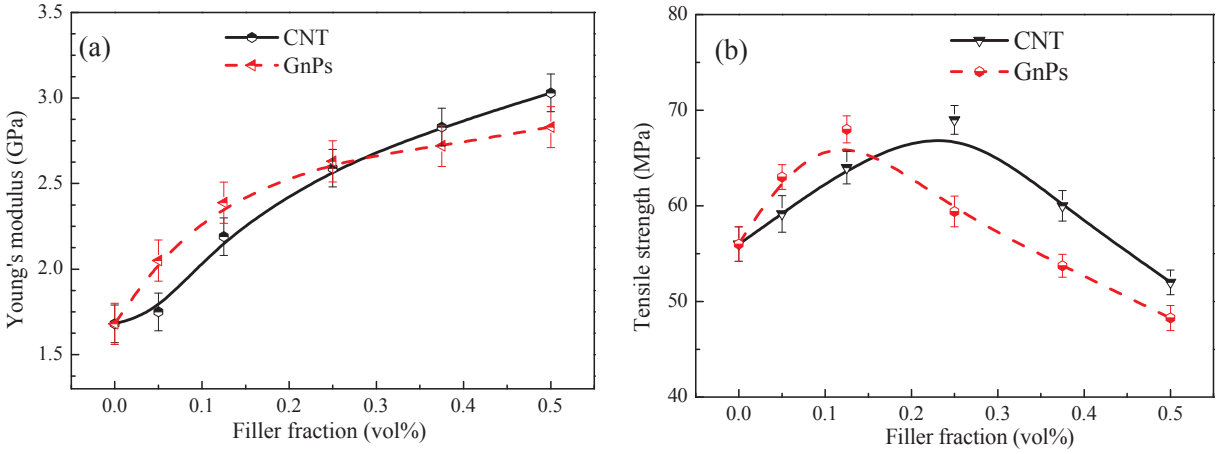

Fig. 3. (a) Young's moduli and (b) tensile strength of the nanocomposite adhesives with different fillers.

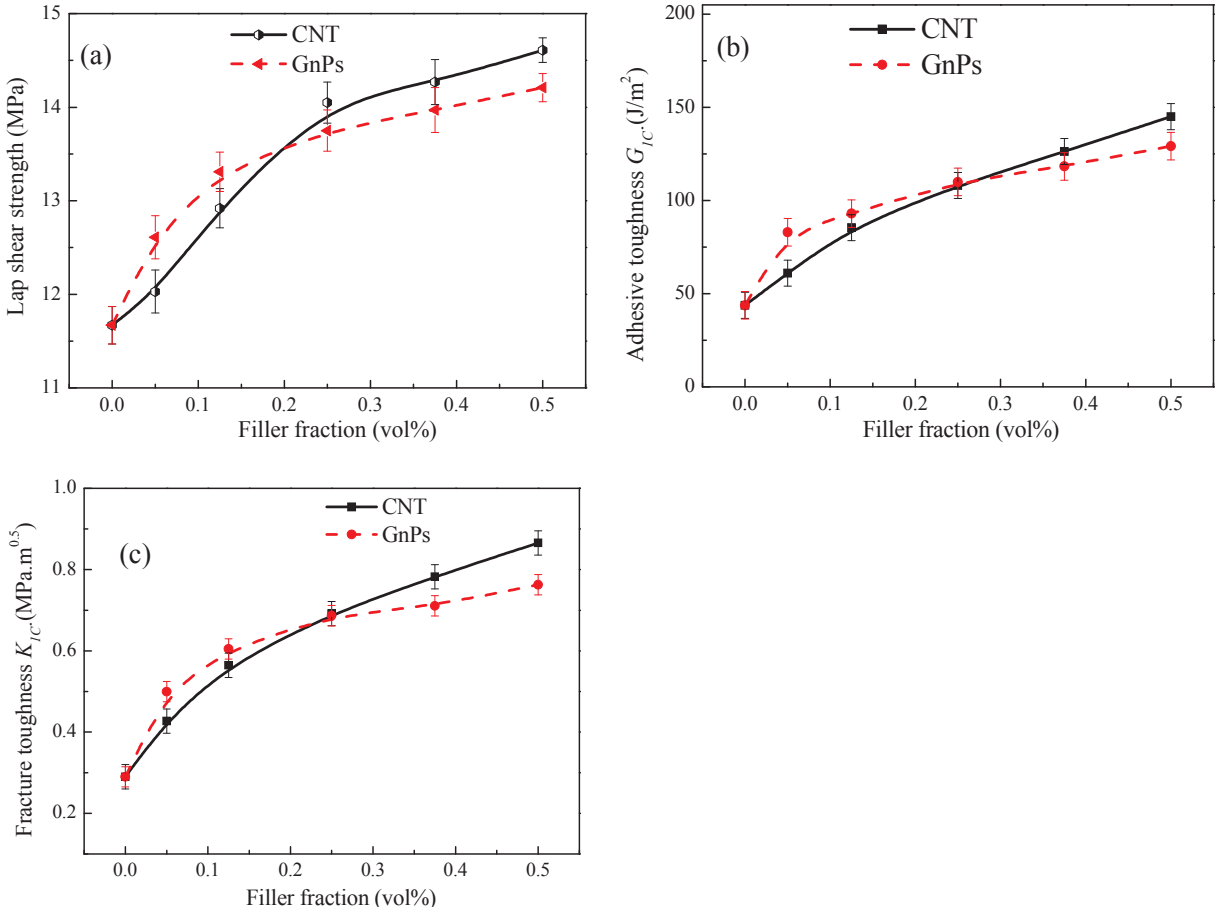

Fig. 4. (a,b) Lap shear strength and energy release rate (G_{IC}) of nanocomposite adhesives respectively, and (c) fracture toughness (K_{IC}) of epoxy/GnP and CNT nanocomposites.

begin to degrade. According to the results, this critical fraction varies according to the geometrical structure of the nanofiller (plate-like structure and tube-like structure). Mechanical reinforcement relies on two key factors: (i) uniform dispersion of the reinforcing phase; and (ii) interfacial bonding strength between host matrix and reinforcing phase. At low fraction, both GnPs and CNTs are able to disperse uniformly in epoxy resin. The plate-like structure favors GnP an advantage to possess strong interfacial bonding with epoxy matrix compare tube-like structure of CNTs. Also, as supported by SEM, GnPs has corrugated surface where mechanical interlocking occurs. Therefore, GnPs result in effective stress transfer between GnPs and epoxy.

At high fraction, GnPs stack to each other forming clusters and CNTs agglomerate. However, the contrast in geometrical structure between the two carbon fillers results different responses in epoxy composites. The schematic presented in Fig. 5 explains the reinforcement at high fraction relying on rigidity of filler network formed inside the matrix. CNTs have extraordinarily high aspect ratio (up to 1000) which enables them to form global, rigid and strong network inside the matrix resisting the applied load and showing high Young's moduli. On the other, GnPs stack to each other forming loose network compare to CNTs. This explains the rapid rate of declining which is experienced at high vol% of GnPs. Images of epoxy/GnP and epoxy/CNT nanocomposites at 0.125 and 0.5 vol% were captured by transmission electron microscopy (TEM) to confirm our hypothesis in Fig. 6. Image (a) displays that at low fraction CNTs are dispersed evenly in the epoxy matrix with a loose network while image (b) reveals that CNTs are entangled and overlapped forming rigid and global network owing to its high aspect ratio. Images (c) and (d) present the dispersion of GnPs in epoxy matrix at low and high fractions respectively. Image (c) presents fine and uniform dispersion for GnPs while at high fraction (image d) GnPs form clusters and subnetworks indicated by white circles.

3.3. Mechanical properties (numerical analysis)

In this part, a numerical approach is employed to understand and compare the mechanical behavior of carbon-based epoxy adhesives. Three-dimensional Finite Element (FE) model is developed to present a single lap joint (SLJ). The adhesive involved in the joint includes neat epoxy, epoxy/CNT or epoxy/GnP nanocomposite; aluminum alloy (AL6060) was used as adherend material– Fig. 7. Commercial FE analysis software ABAQUS was used for analysis where explicit time integration scheme was chosen to capture sudden failures in the adhesive layer avoiding convergence problems. Since the experiments were carried out quasi-statically, the ratio of kinetic energy to the total energy in the simulations was kept less than 0.5%.

Brick solid (C3D8R) and cohesive (COH3D8) eight noded linear elements were employed for aluminum adherends and the adhesive layer, respectively. A mesh with element size 0.5 × 0.5 × 0.16 mm in the overlap region and a coarser one for the remaining region with a single bias ratio of 3 were used to discretize the adherend material. The dimensions of the elements in the adhesive layer were 0.5 × 0.5 × 0.2 mm. The mesh of the model satisfied the mesh convergency study where the ratio of peak load with respect to the one with a finer mesh (having a half element size in all directions) was less than 5%. The boundary conditions were applied according to the experiment; one end of the SLJ sample was fixed (clamped), while the opposite side was allowed to move only in the direction of loading.

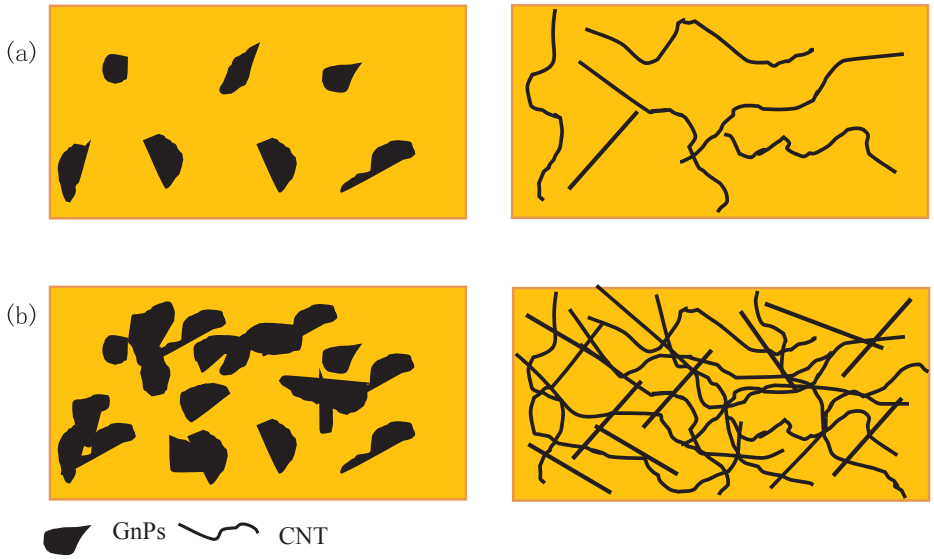

Fig. 5. Graphene platelets (left) and carbon nanotubes (right) in a matrix at (a) low and (b) high volume fractions.

An elastic-plastic material model was used to describe the behavior of the aluminum adherends. Elastic modulus and Poisson's ratio of AL6060 are 69 GPa and 0.35, respectively. Its plastic stress-strain relationship is given in Table 1.

A bilinear cohesive zone model (CZM) was used for the adhesive layer. CZM describes the relation between stresses and corresponding relative displacements, in tension or shear modes. In this model it is assumed that the local zone experiences stresses until reaching a peak values of: traction stress t_n^0 in the normal direction, and t_s^0 and t_t^0 in the first and second shear directions, respectively, describing a linear elastic behavior. The elastic stiffness of the cohesive elements in the normal and shear directions were calculated as the ratio of the elastic and shear modulus to the thickness of the adhesive layer, respectively. The damage initiation refers to the beginning of the degradation of the material following the quadratic nominal stress criterion as follows:

$$\left(\frac{\langle t_n \rangle}{t_n^0}\right)^2 + \left(\frac{t_s}{t_s^0}\right)^2 + \left(\frac{t_t}{t_t^0}\right)^2 = 1 \tag{1}$$

where t_n, t_s and t_t are the traction stresses in the normal (Mode I), first shear (Mode II) and second shear (Mode III) directions, respectively. The Macaulay bracket is used to signify that a pure compressive deformation does not initiate damage. Once the damage initiation criterion is fulfilled, the material damage occurs according to Eq.2:

$$t_i = (1 - D)\bar{t}_i,\ i = n, s, t \tag{2}$$

where D is a scalar damage variable representing the overall damage at a material point, $\bar{t}_i$ are the traction stresses in each direction predicted in the elastic regime without damage. The failure under mixed-mode conditions is governed by a second-order power law as the interaction of the energies required to cause failure in the individual modes as

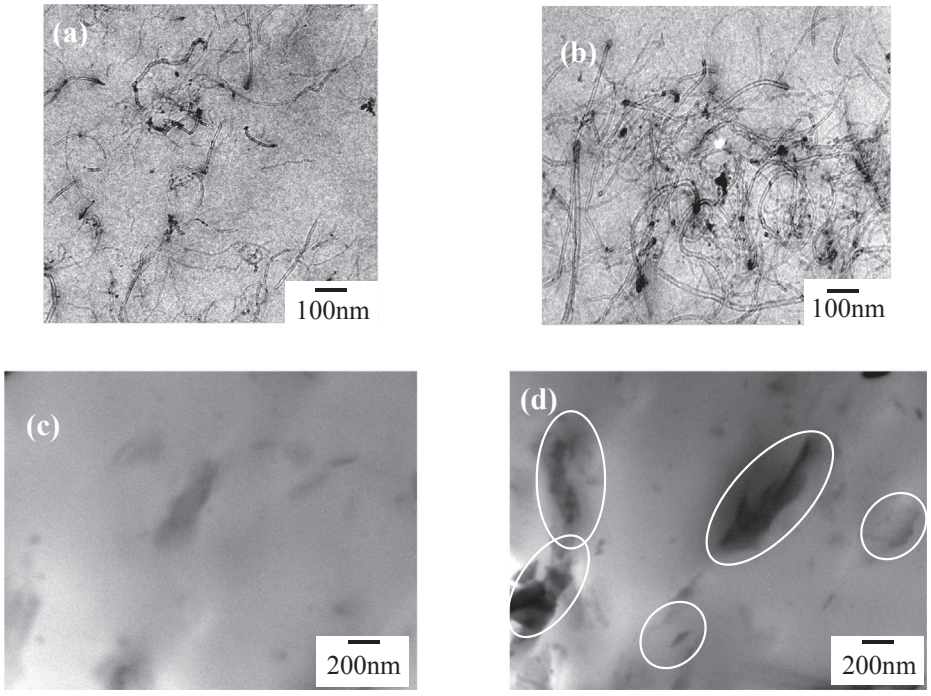

Fig. 6. TEM images of epoxy/CNT composites (a,b) and epoxy/GnP composites (c,d) at 0.125 and 0.5 vol%, respectively.

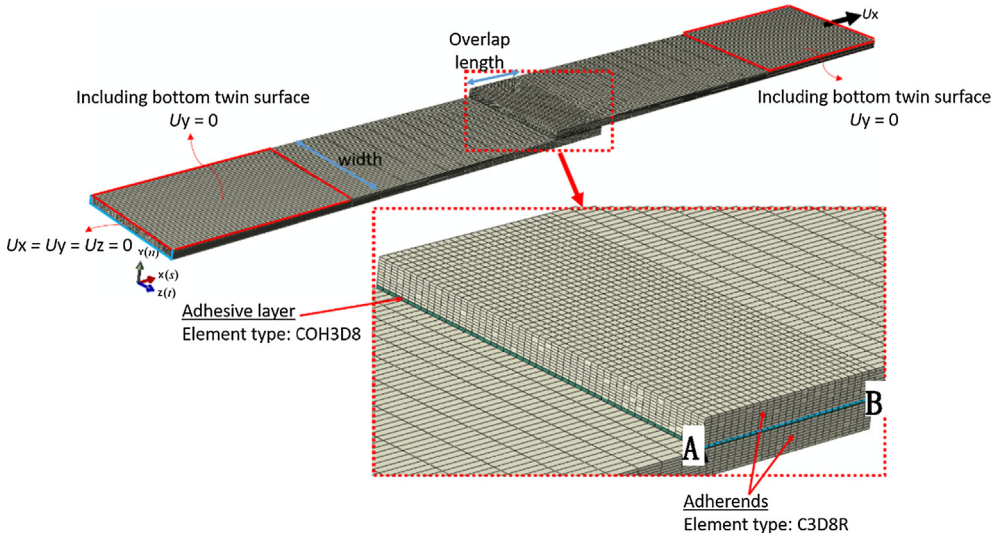

Fig. 7. 3D finite element model of adhesively bonded single lap joint.

Table 1
Stress-strain relationship of AL6060 [39].

Plastic strain	True stress (MPa)
0	203
0.04	232
0.08	241
0.12	250

$$\left(\frac{G_n}{G_n^c}\right)^2 + \left(\frac{G_s}{G_s^c}\right)^2 + \left(\frac{G_t}{G_t^c}\right)^2 = 1 \tag{3}$$

where G_i refer to the work done by the traction and its conjugate relative displacement in the normal, first and second shear directions, respectively. G_n^c, G_s^c and G_t^c are the critical energy release rates for pure Mode I, Mode II and Mode III, respectively. Table 2 presents the material properties of various epoxy nanocomposite adhesives with GnP and CNT employed in the simulations. In the model, the parameters relevant to Mode II and Mode III were considered identical. The values of E, t_n^0, t_s^0 and G_n^c were concluded from Fig. 3. Since the vol% of nanofillers added into epoxy are at low range, the Poisson's ratio (ϑ) was assumed to be the same as of neat epoxy, 0.33 [40]. Based on the isotropy assumption, the shear modulus (G) was calculated using $G = E/2(1 + \vartheta)$, where E is the elastic modulus of the neat adhesive. Since Mode I fracture toughness was only measured herein, the Mode II of fracture toughness (G_s^c) of neat epoxy, epoxy/ GnPs and epoxy/CNTs with 0.5% nanoparticles were taken from the Refs [41,42] while those of 0.05%, 0.125%, 0.250%, 0.375% were obtained by interpolating these values.

Table 2
Material properties of nanocomposite adhesive used in numerical analyses.

		MPa				J/m^2	
	Filler fraction (vol %)	E	G	t_n^0	$t_s^0 = t_t^0$	G_n^c	$G_s^c = G_t^c$
Epoxy/GnP	0.0	1680	631.57	56.00	11.67	43.75	180.00
	0.05	2050	770.67	63.00	12.61	83.00	179.40
	0.125	2388	897.74	68.00	13.31	93.00	178.50
	0.25	2630	988.72	59.41	13.75	110.00	177.00
	0.375	2720	1022.55	53.73	13.97	118.32	175.60
	0.5	2830	1063.91	48.27	14.21	129.20	174.00
Epoxy/CNT	0.00	1680	631.57	56.00	11.67	43.75	180.00
	0.05	1750	657.89	59.16	12.03	61.00	190.00
	0.125	2190	823.30	64.00	12.92	85.42	205.00
	0.25	2590	973.68	69.00	14.05	108.08	230.00
	0.375	2830	1063.91	60.00	14.27	126.29	255.00
	0.5	3030	1139.09	52.00	14.61	145.00	280.00

Fig. 8 presents experimental and numerical values of maximum force obtained from the single lap joints (SLJs) of epoxy nanocomposite adhesives with various contents of GnP and CNT. A reasonably good agreement between them was achieved. Normal (S_{33}) and shear (S_{13}) stress distributions along the overlap length of SLJ (along AB-path, Fig. 7) of the neat adhesive is shown in Fig. 9. It was noticed that the values of the second shear stress (S_{23}) were not significant; thus, they were not presented. It is clear that the S_{33} is maximum near the edges

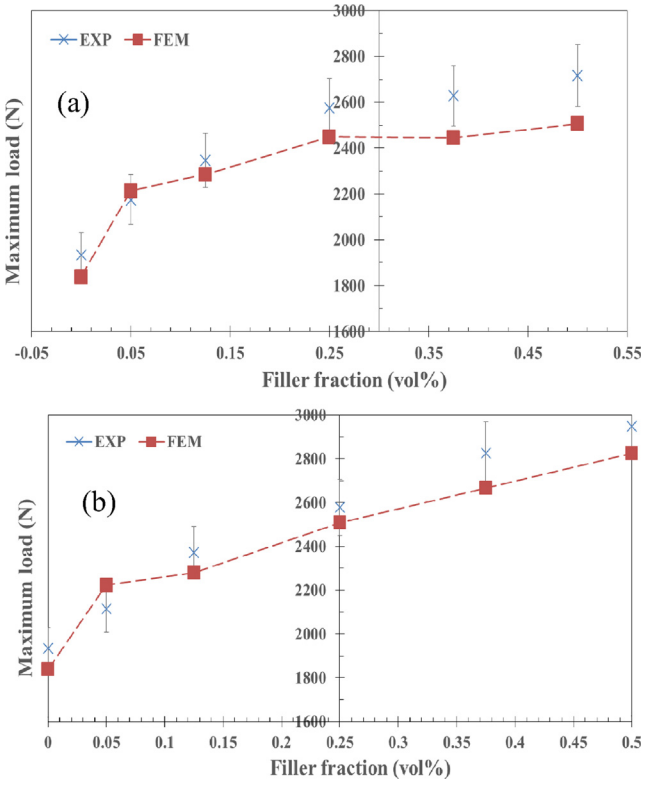

Fig. 8. Experimentally and numerically obtained maximum load values from the SLJs of adhesives with different vol. % of GnP (a) and CNT (b) fillers.

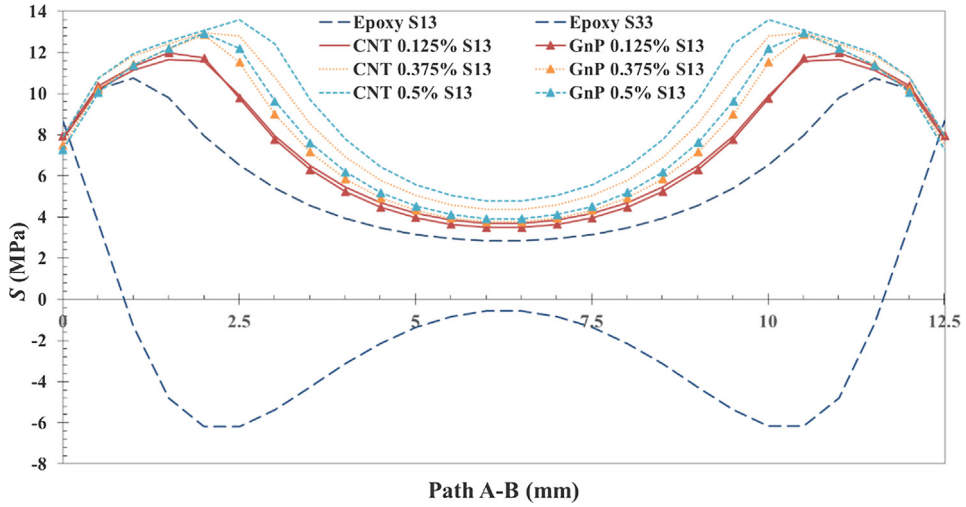

Fig. 9. S_{13} values along path A-B (see Fig. 7) for the SLJs made from nanocomposite adhesives with different vol% of GnP and CNT fillers, and S_{33} for the neat adhesive (Epoxy).

and minimum at the centre, whereas maximum value of S13 is not attained at the edges. The stresses normally reach their maximum at the ends of the overlap length, hence the damage initially appears at these regions; which in turn, led stress values to start decreasing while the stresses in other parts of the overlap length are increasing until the damage starts there. Consequently, the location of maximum stress starts to shift from ends of the overlap length to the mid-part in the course of deformation [43]. However, here, this is valid only for the shear stress, but not for the normal stress as the peeling stresses at the edges did not reach to the critical stress as opposed to the case for the first in-plane shear stress due to the fact that t_n^0 values are around 4 times larger than t_s^0 values. Therefore, the peeling stresses cannot reach to the t_n^0, while the first in-plane shear stresses are reaching to the t_s^0. We here concluded that the failure in the epoxy adhesive layer with CNT or GnP occurred due to only Mode II failure. That also explains the reason for the increase in the maximum force value with an increase in the volume content of the nanofillers observed in Fig. 8. As the t_s^0 is an important parameter here to define the onset damage in the adhesive layer, its value is directly related to maximum force obtained in Fig. 3(a). On the other hand, as the Mode II was not activated in the failure of the adhesive, t_n^0 had very limited effect on the maximum load, hence its variation for different percentage of fillers was not reflected.

The shear stress distributions along path AB for the adhesives having 0.125%, 0.375% and 0.5% of GnP and CNT are presented in Fig. 9. It was observed that with the increase of vol% of GnP or CNT, not only the value of the maximum shear stress increased, but also its location shifted with a larger amount from the edges towards the center, i.e. more surface area was exposed to the damage before the failure of the SLJ. Since t_s^0 is getting higher at large vol%, the material can withstand higher shear stresses, hence their SLJ samples carry higher tensile forces.

When the shear strength of the adhesive layer with the same volume content of GnP and CNT were compared, they were closer to each other at 0.125 vol%, but larger for CNT at 0.375 and 0.5 vol% as in accord with the change *in* t_s^0. It should be emphasized that the critical energy release rate for Mode II (G_s^c) of an adhesive layer also influenced the failure behaviour of the SLJ; at high G_s^c, the adhesive layer experienced long failure displacement. With the increase in GnP vol%, G_s^c slightly dropped while it increased in case of CNT (see Table 2). This explains the large gap between the maximum force values at high volume fraction of GnP and CNT as well as the shear strength explained above.

3.4. Fracture surface (SEM)

The failure of nanocomposite adhesive is a complicated process and involves the loss of structural integrity at microscopic and macroscopic levels under deformation. The fracture surface of compact tension (CT) specimen provides critical information in identifying fracture and toughening mechanisms for nanocomposite adhesive. The fracture surfaces of nanocomposite adhesive were investigated by scanning electron microscopy (SEM) and the micrographs are shown in Fig. 10 and Fig. 11. Since the neat epoxy adhesive fracture surface is well known for being relatively smooth and mirror-like feature [44–46], its SEM micrographs are not shown in this study.

Fig. 10(a1) shows surface fractography analysis of the 0.125 vol% epoxy/GnP nanocomposite adhesive. A typical region at the crack tip (known as stress-whitened zone) is magnified in Fig. 10(a2), which indicates well-dispersed platelets of low thickness in the matrix. The fracture surface demonstrates a number of voids and layer breakage as shown in Fig. 10(a3), a typical phenomenon in toughened epoxy. SEM elemental analysis shows these microcracks occurred in GnPs rather than the matrix which might be due to GnP delamination during fracture process. All these fracture phenomena, including voids, layer breakage and microcracks, occurred in the dispersion phase–GnPs, consuming fracture energy.

Fig. 10(b1) contains the CT fracture surface of the 0.125 vol% epoxy/CNT nanocomposite adhesive. A randomly selected region is magnified in Fig. 10(b2), the fracture surface exhibits relatively rough with some river-like structures (Fig. 10b2). A number of river-lines (indicated by red arrows), which were produced by loading and are usually observed on insufficiently toughened fracture-surfaces, are found in front of plastic deformation zone. When a typical zone is magnified in Fig. 10(b3) microcracks are observed, which means consuming fracture energy.

Comparatively, the nanocomposite adhesive with low GnPs loading exhibits a rougher fracture surface (Fig. 10a2), and numerous tortuous and fine river-like structures with hackles and ribbons can be observed.

Fig. 11(a1) shows an overview of the fractography of 0.5 vol% epoxy/GnP nanocomposite adhesive where a typically rough surface with an obvious deformation zone of ~1.7 mm in length, indicating energy absorbed during crack propagation. A randomly selected region is magnified in Fig. 11(a2), few pull-outs are observed as indicated by white arrows, and this means GnPs likely forming either aggregates or clusters in the matrix as a result of imperfect dispersion of GnPs in nanocomposite adhesive. Fig. 11(a3) illustrates a magnified region of plastic deformation zone. For a well-balanced energy consumption

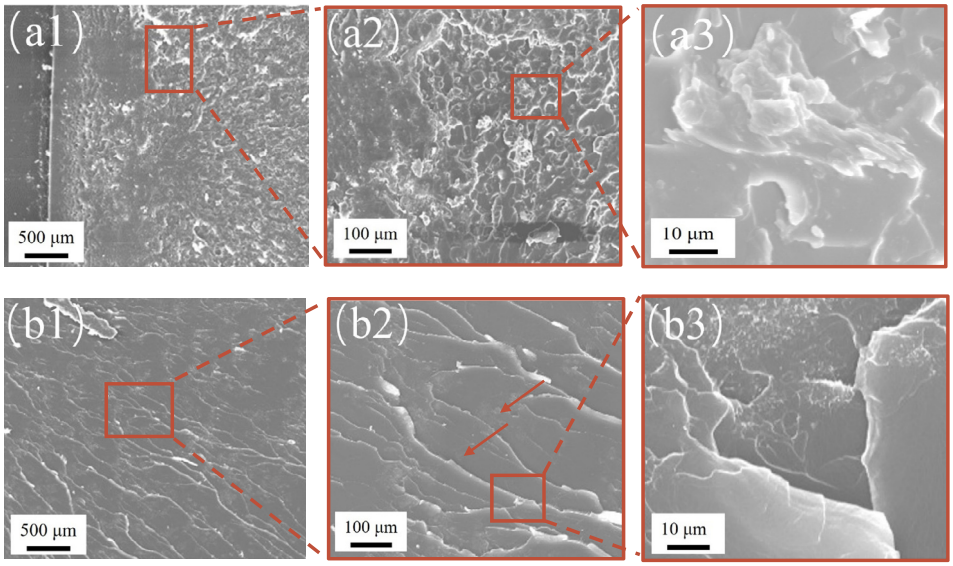

Fig. 10. (a1–a3) epoxy/GnP nanocomposite adhesives and (b1–b3) epoxy/CNT nanocomposite adhesives at 0.125 vol%.

fractured surface, the famous regular river-lines and scale-liked patterns, which were produced by loading are typically observed [47,48]. However, a number of irregular whitening bands and lines are observed in Fig. 11(a3), which represent unbalanced energy absorption and consumption on the fractured surfaces. This means that GnPs may form either aggregates or clusters in the matrix as a result of relatively imperfect dispersion of additives in composite adhesives. During fracture, these lines carried high level of loading and thus experienced high deformation where appeared lighter than other areas promoting dilatation. Dilatation refers to an expansion in volume of a material under stress, which appears lighter or brighter under SEM.

Fig. 11(b1-b3) show SEM micrographs of the fracture surface of 0.5 vol% epoxy/CNT nanocomposite adhesive. Fig. 11(b1) exhibits a rougher fracture surface (Fig. 11b2), and numerous tortuous and fine river-like structures with hackles and ribbons can be observed (white arrows) and demonstrates the following features different to the 0.5 vol % epoxy/GnP nanocomposite adhesive. First, a longer prorogation zone (plastic deformation zone) of ~16.6 mm in length is seen in front of a crack tip, implying a higher level of energy release. Second, no obvious whitening bands and clustered structures, although these two phenomena dominate in Fig. 11(a1); only thin whitening lines can be observed implying better stress distribution under loading. Therefore, the crack under loading propagates far more uniformly and steadily. Normally, the improved surface roughness is accompanied by the creation of matrix plastic deformation, and thus much fracture energy is likely dissipated [44,49]. Finally, highly deformed or fractured CNTs are observed as circles by red dash-line in Fig. 11(b3), which explains why 0.5 vol% CNTs increased the energy release rate G_{1C} significantly than 0.5 vol% GnPs. Therefore, the high CNT loading (> 0.25 vol%) in matrix could lead to an increase of the energy dissipation during the fracture process and a higher fracture toughness value as shown in Fig. 3b.

3.5. Electrical conductivity

Most of polymers – including epoxy – are considered as electrically non-conductive materials. Electrical conductivity of ~ 10^{-6} S·cm^{-1} is adequate in anti-static applications [50] which is indispensable in many applications such as aerospace and mining industry. Since epoxy adhesives are extensively used in aerospace and electronic

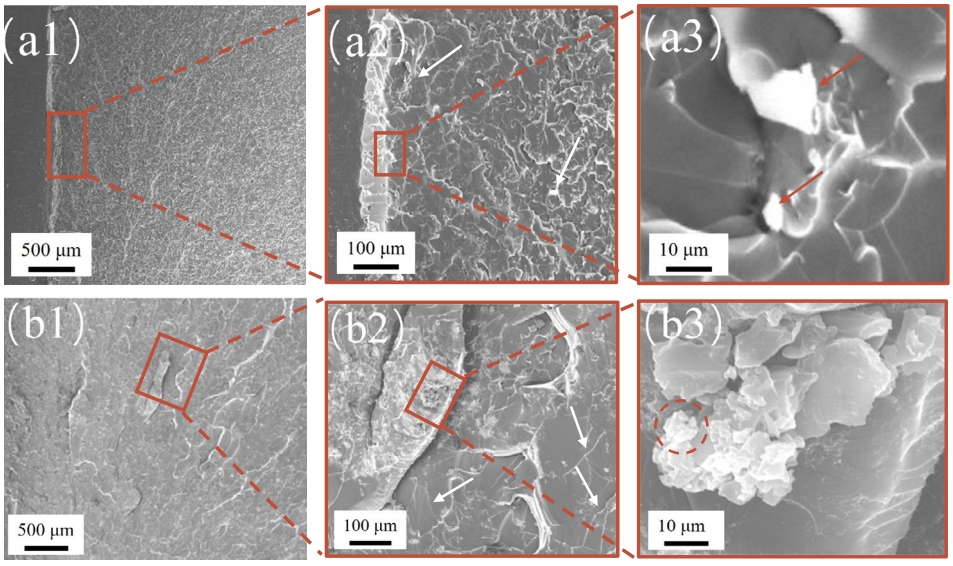

Fig. 11. (a1–a3) epoxy/GnP nanocomposite adhesives and (b1–b3) epoxy/CNT nanocomposite adhesives at 0.5 vol%.

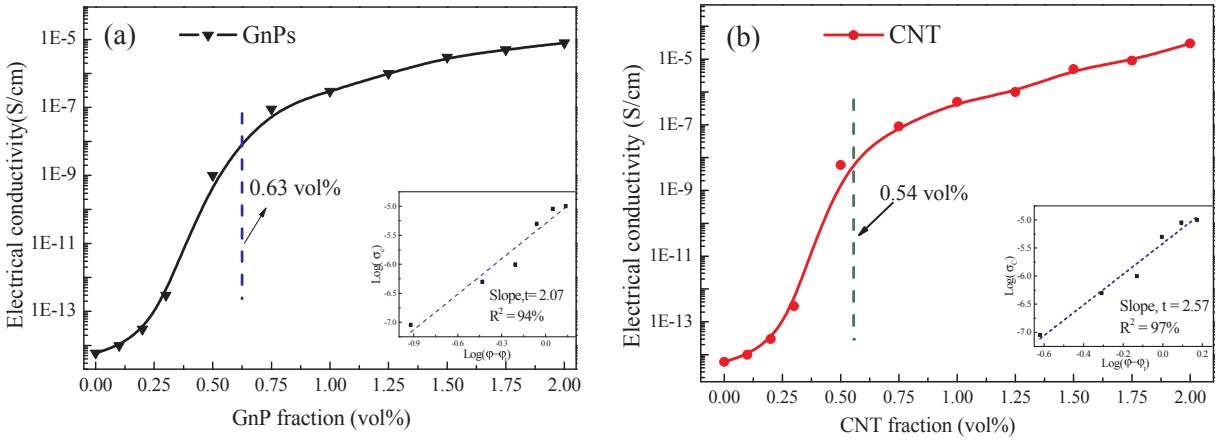

Fig. 12. Electrical conductivity of epoxy/GnP and CNT nanocomposite adhesives.

industries, it is essential to promote their electrical conductivity to match the requirements of such applications. Conductive fillers including metal-based particles and carbon-based materials are commonly incorporated into epoxy adhesives to improve their electrical conductivity. In comparison to graphene oxide and reduced graphene oxide, the yielded GnPs features high structural integrity leading to high electrical conductivity of 1460 $S{\cdot}cm^{-1}$ [31]; range of thickness 3–5 nm offering large surface area giving strong interface for stress, heat and electron transfer with epoxy matrix; epoxide groups existing on GnPs' surface which can chemically react with the end-amine groups of organic molecules building strong interface for the nanocomposite adhesives; and most important cost-effectiveness (~ $20/kg).

The electrical conductivity of the nanocomposite adhesive as a function of GnP and CNT contents is shown in Fig. 12a and b. The results show that both GnPs and CNTs have dramatically promoted the electrical conductivity of the epoxy nanocomposites; at 2 vol%, the epoxy/GnP nanocomposite adhesive show an electrical conductivity of 8×10^{-6} $S{\cdot}cm^{-1}$, which is an increase of ~ 8 orders of magnitude over the conductivity of the neat epoxy adhesive; epoxy/CNT nanocomposite adhesive owns better performance with electrical conductivity of 3×10^{-5} $S{\cdot}cm^{-1}$, an increase of 9 orders of magnitude. These results confirm that GnPs and CNTs are excellent conductive fillers for epoxy adhesive at low concentration loadings. Also, Fig. 12 concludes that at 0.5 vol%, the conductive fillers (GnPs and CNTs) start to contact each other forming networks which constitutes of continuous paths for electrons mobility resulting in high electrical conductivity. It is clear that percolation threshold lays between 0.25 and 0.75 vol% for both fillers. In general, electrical conductivity of polymer composites relies on the intrinsic electrical conductivity of second phase, its dispersion quality and aspect ratio. To possess better understanding, further analysis is carried out by fitting the experimental data into the power law equation:

$$\sigma_c = \sigma_f(\varphi - \varphi_t)^t \quad (4)$$

where σ_c and σ_f are the conductivity of nanocomposite and filler (GnPs or CNTs), respectively; φ is the filler vol%; φ_t is the percolation threshold and t is the critical exponent. The percolation threshold is known to be largely reliant on the microstructure of the conductive filler, whereas the critical exponent t depends only on system dimensionality [51]. The fitting line for the experimental results is shown in Fig. 12 inset. Percolation thresholds of about 0.54 vol% and 0.63 vol % are observed respectively for epoxy/GnP and epoxy/CNT systems and were calculated based on the best fit to the experimental results.

It is worth noting that the critical exponent t = 2.57 of epoxy/CNT nanocomposite adhesive is higher than the critical exponent t = 2.07 of the epoxy/GnP nanocomposite adhesive, indicative of a CNT filler network closer to the 3D type architecture. In the CNT filled system, the conductive network was formed at a lower vol% than GnPs filled systems due to the high aspect ratio of CNT, refer to Fig. 5.

4. Conclusions

Graphene platelets and carbon nanotubes were selected and filled epoxy adhesives in order to develop high mechanical performance and electrically conductive adhesives. Structure-property relations of both systems (epoxy/GnP and epoxy/CNT) were experimentally and numerically compared and investigated. The results clearly indicate that the GnPs and CNT nanofiller can improve the performance of epoxy adhesive. The maximum improvement in tensile strength was 20% with 0.125 vol% GnPs and 23% with 0.25 vol% CNT, on further increasing the filler loading, there was a sharp decrement in tensile strength. Also, the study depicted that GnPs provides better improvement in Young's modulus, lap shear strength and G_{1C} than CNT at low fractions ($<$ 0.25 vol%) while CNT proves better reinforcement than GnPs at high loading ($>$ 0.25 vol%). The Young's modulus, lap shear strength and G_{1C} were increased by 80%, 25% and 231% at 0.5 vol% CNT, while these properties were increased by 68%, 22% and 195% at the same fraction of GnPs, respectively. The main active toughening mechanisms were crack pinning, crack deflection, and crack bridging. For further investigation, a numerical model was built using a bilinear cohesive zone model (CZM). It was observed that with an increase in GnP or CNT vol%, a larger surface area of the adhesive layer was exposed to damage before failure, hence the respective single lap joint samples showed a better mechanical performance by carrying higher tensile forces.

A percolation threshold of electrical conductivity was found at 0.63 vol% GnPs; while a low percolation threshold of 0.54 vol% for epoxy/CNT nanocomposite adhesive. The contrast in geometrical structure between the two carbon fillers results different responses in epoxy composites. The results indicate that CNT as a structural reinforcement additive is more effective than GnP at high loading, which contributes to the formation of rigid network of CNT.

Acknowledgement

QM thanks Asbury and Huntsman (China) for providing the graphite intercalation compounds (1395) and Jeffamine D230, respectively. This work was financially supported by the Natural Science Foundation of Liaoning Province, China (20170520142). Dr. Tianqing Liu is supported by NHMRC Early Career Fellowship (1112258).

References

[1] Lu S, Tian C, Wang X, Chen D, Ma K, Leng J, et al. Health monitoring for composite materials with high linear and sensitivity GnPs/epoxy flexible strain sensors. Sens Actuat A: Phys 2017;267:409–16.

[2] Messina E, Leone N, Foti A, Di Marco G, Riccucci C, Di Carlo G, et al. Double-wall nanotubes and graphene nanoplatelets for hybrid conductive adhesives with enhanced thermal and electrical conductivity. ACS Appl Mater Interf 2016;8(35):23244–59.

[3] Gong L-X, Zhao L, Tang L-C, Liu H-Y, Mai Y-W. Balanced electrical, thermal and mechanical properties of epoxy composites filled with chemically reduced graphene oxide and rubber nanoparticles. Compos Sci Technol 2015;121:104–14.

[4] Araby S, Saber N, Ma X, Kawashima N, Kang H, Shen H, et al. Implication of multi-walled carbon nanotubes on polymer/graphene composites. Mater Des (1980–2015) 2015;65:690–9.

[5] Mannov E, Schmutzler H, Chandrasekaran S, Viets C, Buschhorn S, Tölle F, et al. Improvement of compressive strength after impact in fibre reinforced polymer composites by matrix modification with thermally reduced graphene oxide. Compos Sci Technol 2013;87:36–41.

[6] Geim AK. Graphene:Status and Prospects. International of Vacuum Congress2010. p. 1530.

[7] Yu MF, Files BS, Arepalli S, Ruoff RS. Tensile loading of ropes of single wall carbon nanotubes and their mechanical properties. Phys Rev Lett 2014;84(3–4):5552–5.

[8] Araby S, Meng Q, Zhang L, Zaman I, Majewski P, Ma J. Elastomeric composites based on carbon nanomaterials. Nanotechnology. 2015;26(11):112001.

[9] Sengupta R, Bhattacharya M, Bandyopadhyay S, Bhowmick AK. A review on the mechanical and electrical properties of graphite and modified graphite reinforced polymer composites. Prog Polym Sci 2011;36(5):638–70.

[10] Yu MF, Lourie O, Dyer MJ, Moloni K, Kelly TF, Ruoff RS. Strength and breaking mechanism of multiwalled carbon nanotubes under tensile load. Science 2000;287(5453):637–40.

[11] Al-Saleh MH, Sundararaj U. A review of vapor grown carbon nanofiber/polymer conductive composites. Carbon 2009;47(1):2–22.

[12] Volder MFLD, Tawfick SH, Baughman RH, Hart AJ. Carbon nanotubes: present and future commercial applications. Science 2013;339(6119):535–9.

[13] Tang L-C, Wan Y-J, Peng K, Pei Y-B, Wu L-B, Chen L-M, et al. Fracture toughness and electrical conductivity of epoxy composites filled with carbon nanotubes and spherical particles. Compos A Appl Sci Manuf 2013;45:95–101.

[14] Shi G, Araby S, Gibson CT, Meng Q, Zhu S, Ma J. Graphene platelets and their polymer composites: fabrication, structure, properties, and applications. Adv Funct Mater 2018;28(19):1706705.

[15] Li X, Chen Y, Cheng Z, Jia L, Mo S, Liu Z. Ultrahigh specific surface area of graphene for eliminating subcooling of water. Appl Energy 2014;130:824–9.

[16] K. S. Novoselov AKG, 1* S. V. Morozov,2 D. Jiang,1, Y. Zhang SVD, 2 I. V. Grigorieva,1 A. A. Firsov2. Electric Field Effect in Atomically Thin Carbon Films. 2004.

[17] Araby S, Li J, Shi G, Ma Z, Ma J. Graphene for flame-retarding elastomeric composite foams having strong interface. Compos A Appl Sci Manuf 2017;101:254–64.

[18] Araby S, Qiu A, Wang R, Zhao Z, Wang C-H, Ma J. Aerogels based on carbon nanomaterials. J Mater Sci 2016;51(20):9157–89.

[19] Sydlik SA, Lee J-H, Walish JJ, Thomas EL, Swager TM. Epoxy functionalized multi-walled carbon nanotubes for improved adhesives. Carbon 2013;59:109–20.

[20] Moriche R, Prolongo SG, Sánchez M, Jiménez-Suárez A, Chamizo FJ, Ureña A. Thermal conductivity and lap shear strength of GNP/epoxy nanocomposites adhesives. Int J Adhes Adhes 2016;68:407–10.

[21] Jakubinek MB, Ashrafi B, Zhang Y, Martinez-Rubi Y, Kingston CT, Johnston A, et al. Single-walled carbon nanotube–epoxy composites for structural and conductive aerospace adhesives. Compos B Eng 2015;69:87–93.

[22] Bisht A, Dasgupta K, Lahiri D. Effect of graphene and CNT reinforcement on mechanical and thermomechanical behavior of epoxy-A comparative study. J Appl Polym Sci 2018;135(14):46101.

[23] Chatterjee S, Wang JW, Kuo WS, Tai NH, Salzmann C, Li WL, et al. Mechanical reinforcement and thermal conductivity in expanded graphene nanoplatelets reinforced epoxy composites. Chem Phys Lett 2012;531:6–10.

[24] Oh H, Kim K, Ryu S, Kim J. Enhancement of thermal conductivity of polymethyl methacrylate-coated graphene/epoxy composites using admicellar polymerization with different ionic surfactants. Compos A Appl Sci Manuf 2019;116:206–15.

[25] Mahmood H, Vanzetti L, Bersani M, Pegoretti A. Mechanical properties and strain monitoring of glass-epoxy composites with graphene-coated fibers. Compos A Appl Sci Manuf 2018;107:112–23.

[26] Han W, Zhang H-P, Tavakoli J, Campbell J, Tang Y. Polydopamine as sizing on carbon fiber surfaces for enhancement of epoxy laminated composites. Compos Part A: Appl Sci Manufact 2018;107:626–32.

[27] Yang S-Y, Lin W-N, Huang Y-L, Tien H-W, Wang J-Y, Ma C-CM, et al. Synergetic effects of graphene platelets and carbon nanotubes on the mechanical and thermal properties of epoxy composites. Carbon 2011;49(3):793–803.

[28] Wernik JM, Meguid SA. On the mechanical characterization of carbon nanotube reinforced epoxy adhesives. Mater Des 2014;59:19–32.

[29] Li S, Liu X, Fang C, Liu N, Liu D. Surface modification and thermal performance of a graphene oxide/novolac epoxy composite. RSC Adv 2018;8(37):20505–16.

[30] Naebe M, Wang J, Amini A, Khayyam H, Hameed N, Li LH, et al. Mechanical property and structure of covalent functionalised graphene/epoxy nanocomposites. Sci Rep 2014;4:4375.

[31] Meng Q, Jin J, Wang R, Kuan HC, Ma J, Kawashima N, et al. Processable 3-nm thick graphene platelets of high electrical conductivity and their epoxy composites. Nanotechnology 2014;25(12):125707.

[32] Ghaleb ZA, Mariatti M, Ariff ZM. Properties of graphene nanopowder and multi-walled carbon nanotube-filled epoxy thin-film nanocomposites for electronic applications: the effect of sonication time and filler loading. Compos A 2014;58(3):77–83.

[33] Chatterjee S, Nafezarefi F, Tai NH, Schlagenhauf L, Nüesch FA, Chu BTT. Size and synergy effects of nanofiller hybrids including graphene nanoplatelets and carbon nanotubes in mechanical properties of epoxy composites. Carbon 2012;50(15):5380–6.

[34] Li W, Dichiara A, Bai J. Carbon nanotube–graphene nanoplatelet hybrids as high-performance multifunctional reinforcements in epoxy composites. Compos Sci Technol 2013;74:221–7.

[35] Owais M, Zhao J, Imani A, Wang G, Zhang H, Zhang Z. Synergetic effect of hybrid fillers of boron nitride, graphene nanoplatelets, and short carbon fibers for enhanced thermal conductivity and electrical resistivity of epoxy nanocomposites. Compos A Appl Sci Manuf 2019;117:11–22.

[36] Chen B, Li X, Jia Y, Xu L, Liang H, Li X, et al. Fabrication of ternary hybrid of carbon nanotubes/graphene oxide/MoS2 and its enhancement on the tribological properties of epoxy composite coatings. Compos A Appl Sci Manuf 2018;115:157–65.

[37] Chandrasekaran S, Faiella G, Prado LASA, Tölle F, Mülhaupt R, Schulte K. Thermally reduced graphene oxide acting as a trap for multiwall carbon nanotubes in bi-filler epoxy composites. Compos Part A: Appl Sci Manufact 2013;49:51–7.

[38] Zaman IK, Dai HC, Kawashima J, Michelmore N, Sovi A, Dong A, et al. From carbon nanotubes and silicate layers to graphene platelets for polymer nanocomposites. Nanoscale 2012;4(15):4578–86.

[39] Chen Y, Clausen AH, Hopperstad OS, Langseth M. Stress–strain behaviour of aluminium alloys at a wide range of strain rates. Int J Solids Struct 2009;46(21):3825–35.

[40] Kim M, Park Y-B, Okoli OI, Zhang C. Processing, characterization, and modeling of carbon nanotube-reinforced multiscale composites. Compos Sci Technol 2009;69(3):335–42.

[41] Quan D, Urdániz JL, Ivanković A. Enhancing mode-I and mode-II fracture toughness of epoxy and carbon fibre reinforced epoxy composites using multi-walled carbon nanotubes. Mater Des 2018;143:81–92.

[42] Domun N, Hadavinia H, Zhang T, Sainsbury T, Liaghat GH, Vahid S. Improving the fracture toughness and the strength of epoxy using nanomaterials – a review of the current status. Nanoscale 2015;7(23):10294–329.

[43] Demiral M, Kadioglu F. Failure behaviour of the adhesive layer and angle ply composite adherends in single lap joints: a numerical study. Int J Adhes Adhes 2018;87:181–90.

[44] Le Q-H, Kuan H-C, Dai J-B, Zaman I, Luong L, Ma J. Structure–property relations of 55 nm particle-toughened epoxy. Polymer 2010;51(21):4867–79.

[45] Ma J, Mo MS, Du XS, Dai SR, Luck I. Study of epoxy toughened by in situ formed rubber nanoparticles. J Appl Polym Sci 2008;110(1):304–12.

[46] Kuan HC, Dai JB, Ma J. A reactive polymer for toughening epoxy resin. J Appl Polym Sci 2010;115(6):3265–72.

[47] Hull D. Fractography: Observing. Measuring and Interpreting Fracture Surface Topography: Cambridge University Press; 1999.

[48] Ma J, Mo MS, Du XS, Rosso P, Friedrich K, Kuan HC. Effect of inorganic nanoparticles on mechanical property, fracture toughness and toughening mechanism of two epoxy systems. Polymer 2008;49(16):3510–23.

[49] Zhang H, Tang LC, Zhang Z, Friedrich K, Sprenger S. Fracture behaviours of in situ silica nanoparticle-filled epoxy at different temperatures. Polymer 2008;49(17):3816–25.

[50] Ma PC, Siddiqui NA, Marom G, Kim JK. Dispersion and functionalization of carbon nanotubes for polymer-based nanocomposites: a review. Compos A 2010;41(10):1345–67.

[51] Bauhofer W, Kovacs JZ. A review and analysis of electrical percolation in carbon nanotube polymer composites. Compos Sci Technol 2009;69(10):1486–98.